Chemical characterization of aeolian dust deposition in southern and western Iran

Mansour A. Foroushani *, Christian Opp, Michael Groll

Department of Geography, Philipps-Universität Marburg, D-35037, Germany
** Email Address; mforoushani@gmail.com*

ABSTRACT

In the last decade, the southwestern and western provinces of Iran have been heavily affected by aeolian dust deposition.As a result, the elemental composition of soil surfaces is influenced byaeolian dust transport as well as precipitation, wind speed and direction. The relationship between daily recorded dust eventsandthe elemental composition of the dust are studied in this paper.Strong correlationswere detected between dust deposition rate from most deposition sites(G01-G10, except for G05, G06)and thedust eventfrequency. Correlations of different strengths have been revealed between thedust event frequencies(DEF),and the elemental classification matrix based onAirborne Metal Regulations.

As expected, high correlation values indicate high concentration contributions of elemental values to the aerosol, such as Na, Mn, As, Pb, from large-scale depositions in the south including Cr and V in the west. These findings also suggest that the major contributors of V, Cr, Co, Ni, Cu, Zn, As, Se, Cd, Ba, and Pb in the elemental concentrations may depend on the meteorological situation and correlation magnitude are associated with elements emanating from local anthropogenic activities.

Keywords: Dust composition, ICP-MS, metal concentrations, aeolian dust, Iran

1. INTRODUCTION

Small solid and dry particles below 75 µm in diameter [1] can be projected easily into the air by natural forces[2]andremain suspended in the Earth's atmosphere long enough to substantially affect weather and climate[3].In fact, while particles are airborne, they impact the regional and global climate[4];[5];[6]) and interact with solar and terrestrial radiation, depending on their mineralogical composition, which is determined by the source of deposition [7];[8]).Although natural forces drive dust transport and deposition, dust transport processes can also be substantially constituted through human activities, including off-road driving[9]; [10], land use change[11]; [12];[10];[13]), and anthropogenic activities in general [14];[15]). In the long run, airborne dust is slowly removed from the atmosphere under the influence of gravity, land shape, land cover [16]such as vegetation that can obstruct dust movement effectively[17], and dry deposition, which consists of all deposition that accounts for gravitational settling not associated with precipitation[18]. In a similar manner, airborne particles function as condensation cores in the water cycle [6];[19]and influence soil properties when they are deposited [4]; [5];[20];[21].Aeolian dust can also contribute to the spreading of viruses [22] that also have large-scale effects on the soil, vegetation, animals, and humans [23];[24]; [25],. Aside from immediate threats to the water cycle and soil properties, aeolian dust also causes considerable impairments in social [26]and commercial activities. As a result, the reduced visibility disrupts transport while the subsequent dust can damage engines and technical infrastructure, thus causing severe economic damages [27]; [28]. The sources and impacts of a wide range of chemical compounds have been examined and classified in a range of studies[29];[30];[31], while a comprehensive list of sources compiled for key elements[32] called the Airborne Metals Regulations(AMR) in aeolian particles worldwide (Tab. 1).

Table 1.Key indicating elements with associated sources

Source		Indicating element
Crustal /Geologic	NS	Na, Mg, Al, Si, K, Ca, Mn, Fe, and Sr,
Coal Combustion	DS	Crustal including fine PM such as, As, Se, Ba, and B
Oil combustion	DS	V and Ni
Petroleum Refinery	DS	Elements contained in oil products
Automotive	DS	Br, Pb (fine PM)
Cu, Ni, and Pb Smelter	DS/NS	Cu, As, Cd, Pb
Marine Aerosol	DS/NS	Na
Vegetative Burning	DS/NS	Organic carbon, elemental carbon, K, Zn
Iron and Steel Industry	DS	Fe, Cr, Ni, and Mg (fine PM)

**Example of key indicating elements with associated sources reproduced from Geiger and Cooper (2010)*

According to the Airborne Metals Regulations(AMR), Na, Mg, Al, Si, Ca, Mn, Fe, and Sr are mainly of geologic origin and can thus be classified as coming from natural sources (NS), while elements such as Ni, Br or Pb are mostly associated with industrial and commercial activities, which have been classified as so-called dominant sources (DS)[32].In either case,a detailed knowledge of the dust source and of its activation process, dust event characteristics, dust transport routes, and deposition is crucialto fully understand this complex matter [33].Ultimately, synthesized dust observations need to examine the correlation among atmospheric dust functions,which is invoked the rate of dust deposition and dust event frequency (DEF) relation. Uncertainty has been evaluated for sampling and treatment result after chemical analysis carried out using ICP-MS. Later, attempt to identify the connections between the proximity to potential sources, including NS and DS by means of the element composition. This information is important to understand how anthropogenic activities can directly affect elemental compositionofaeolian particles. The results presented here are the products of a complex study from the west to the southwest of Iranlocated between latitudes 47.101335° and 49.163632°E, longitudes 34.353365° and 30.584651°N.

2. STUDY AREA

Iran is located in Western Asia, between the Oman Seaand the Persian Gulf in the south and the Caspian Sea in the north. Due to its location in an arid region, aeolian dust is a very common phenomenon in Iran, which reaches annual mean concentrations of 50-100 µg/m³ [34]; [35] (Fig. 1-a, b-c).

a-.August 25, 2014, Clear **b-.August, 31, 2014, Clouded** **c-.September 01 2015**

Fig. 1. Satellite imagery over Iran

** The photos are provided by the ISS Crew Earth Observations Facility and the Earth Science and Remote Sensing [Fig. 1 a, b, c][35]. Desert dust in the atmosphere engulfs the Persian Gulf and the western part of Iran [Fig. 1. b, c].*

In addition to information from long term global observations, ten sampling sites were marked (Tab. 2), and the dominant local features were observed. The sites were coded from G01 to G10 and were placed based on the distribution and intensity of the dust events(Fig. 2) reported by [36] between 2009 and 2012. The sampler locations were classified with respect to rural, agricultural, industrial, urban, and suburban areas.

Table 2. Location, altitude and total distance of dust samplers in the research area

			Geo-Coordinate				Distance
No	**Site Classification**	**Code**		**Surrounding environment**	**Altitude(m)**	**Total (Km)**	
1	Rur & Agr & Ind	G01	34.000553,	45.497595	Light Inds & Semi Dessert	144	0	0
2	Sub & Ind	G02	34.007182,	45.499075	Light Inds & Semi Dessert	184	1	1
3	Rur	G03	34.393584,	45.648174	Semi Dessert	394	51	52
4	Agr & Ind	G04	34.423028,	45.993753	Road Traffic Load	910	61	113
5	Urb & Ind	G05	34.353365,	47.101335	Densely occupied	1304	132	245
6	Rur & Agr & Ind	G06	33.024976,	47.759393	Light Inds & village	581	387	632
7	Rur & Agr & Ind	G07	32.380038,	48.282664	Light Inds & village	109	101	733
8	Rur & Agr & Ind	G08	31.445194,	48.632398	Light Inds & village	25	127	860
9	Sub	G09	30.584651,	49.163632	Occupied	6	131	991
10	Urb & Ind	G10	30.352411,	48.292293	Road Traffic Load	2	100	1091

**Dust samplers were coded from G01 to G10. The sampler locations were classified with respect to rural (Rur), agricultural (Agr), industrial (Ind), urban (Urb), and suburban (Sub).*

The study area covers 8.43% of Iran and is located in cold and hot desert climates[37]. The provinces of Khuzestan, Lorestan, and Kermanshah are 64000, 28392, and 24998 (km^2) in area, respectively[38]. In that order, they also play an important role in the country's economy, as they are ranked 2^{nd}, 26^{th} and 21^{st} in Gross Domestic Product (GDP)among Iran's provinces [39]. The censuses indicate that the populations of Khuzestan, Lorestan, and Kermanshah are 4.7, 1.9,and 1.74 million, for a total of 8.34 million[40]. The area's geographic bias information, meteorological data, and climate map adjacent to selecting point will be discussed in the following, as well as in the results and discussion sections.

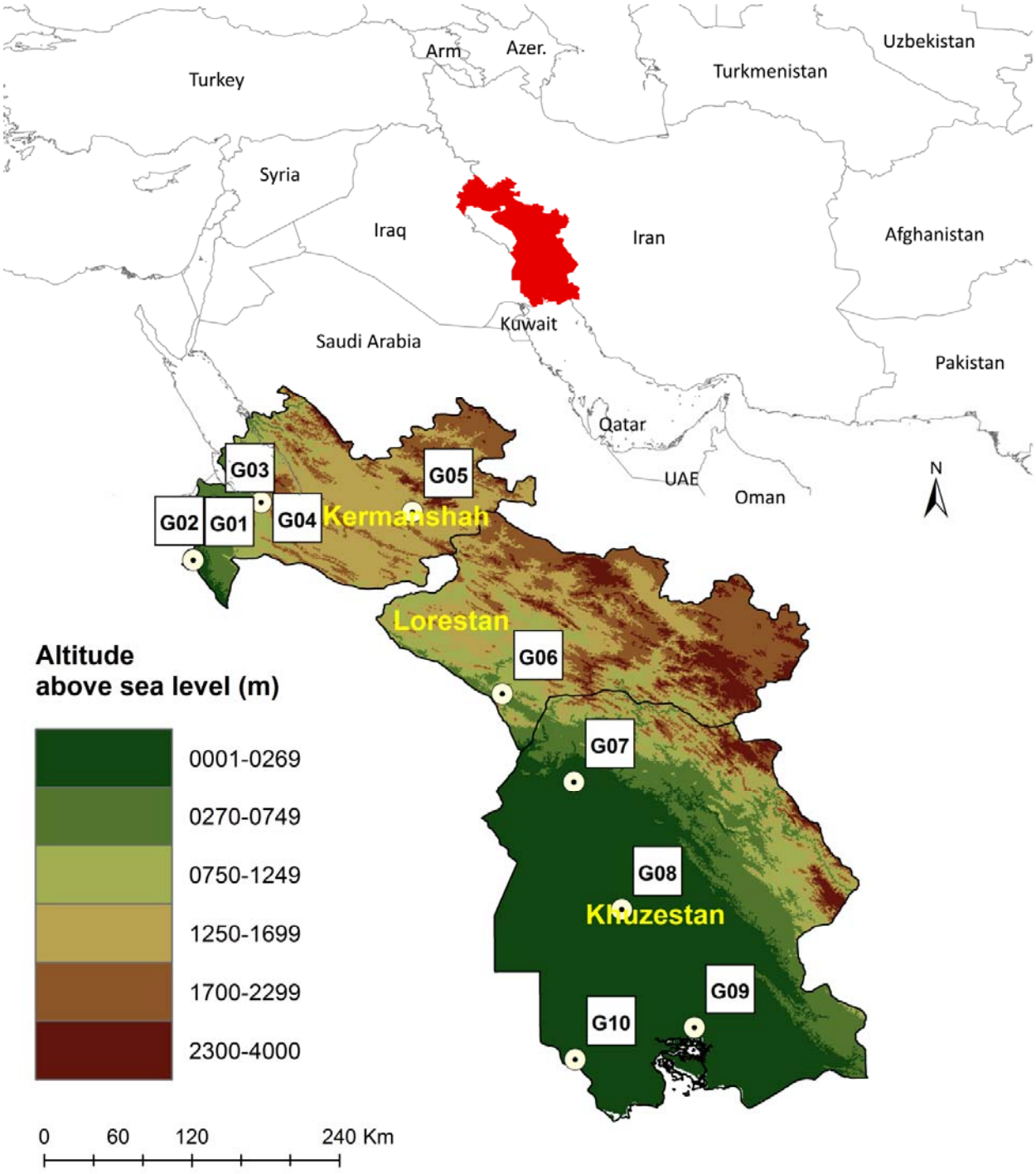

Fig. 2.Mapping gauge sites distribution
**Topo map reproduced from Gt30 NASA EOSDIS [41]*

2.1. Geographic characterization of the research area

A global climate map using the Köppen-Geiger system [37]on the right in Fig. 3 shows the study area being classified as hot desert, hot semiarid and hot summer-Mediterranean. As has been noted, irregular weather patterns, air quality-variant rainfall, and anthropogenic activities have drastically altered the earth's climate in negative ways[42];[43]. The updated field climate mapon the left in Fig. 3 is contains a hot coastal dry climate proportion of 9%, the hot dry desert proportionis 26%, and a strip of hot semidesert area comprises a proportion of 22%, which is extended to the Mediterranean with spring rain for about 35% [44] next to the area of cold mountain climate in the north east. Those are uniquely classified into one climate type by the Köppen-Geiger system (Fig. 3) because of latitude and longitude, monthly precipitation and temperature assessments.

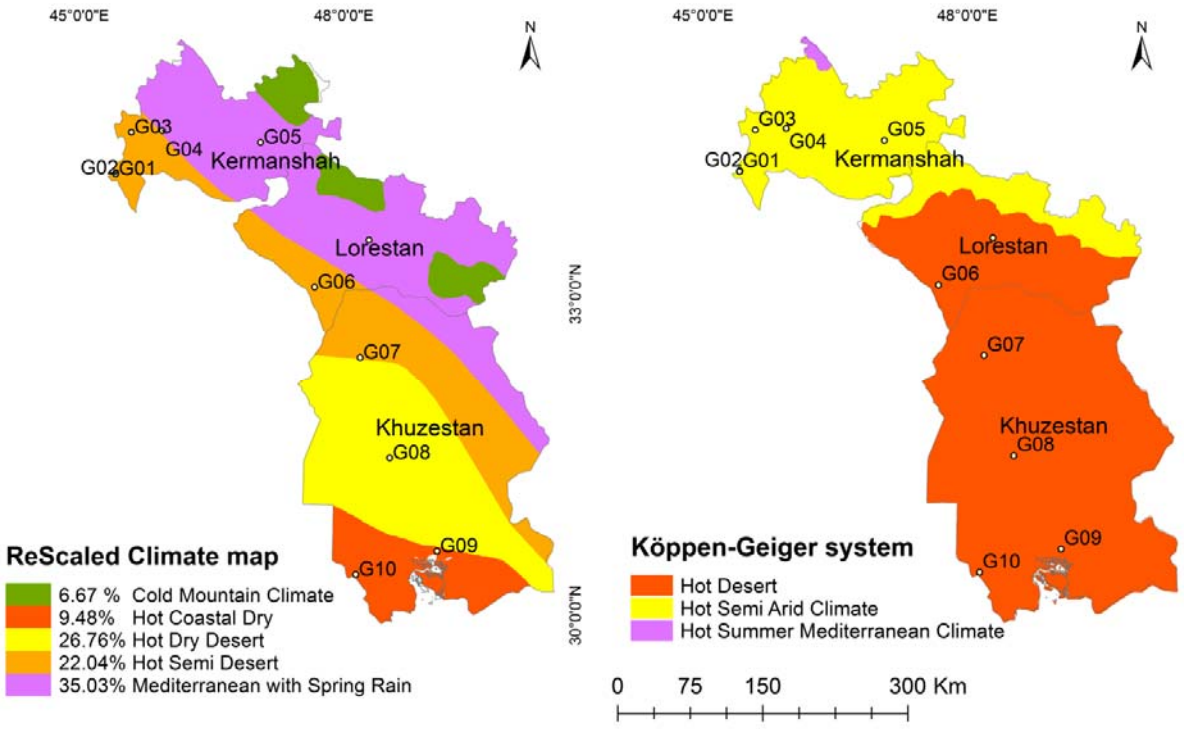

Fig. 3. Rescaled climate map on data from Climatic Zones

**Left (courtesy of Rangeland and Forestry Organization, Tehran; [45]; [46] beside Köppen-Geiger system right*

As Fig. 4 illustrates, the minimum and maximum values of monthly mean precipitation at G10 and G06 are given as 7 (mm) and 26 (mm), respectively (Historical climate data, 2016; [48]. However, precipitation per month notably is below the average in G01. Likely, the precipitation values in G07, G08, and G09 can be classified at the same level below the median value of 15 (mm), thereby extending into G10. In contrast, the rainfall at gauge sites G03, G04, G05, and G06, indicated a value of 19 (mm), which was above average.Ambient monthly temperatures were observed during nearly the entire fieldwork period for maximum and minimum values.The mean temperature during the fieldwork period was generally well above 16(°C). A long period of maximum warm points fluctuated between 29(°C) and 39(°C) in the area of G01, at G02 in the west, and likewise G07, G08, G09, and G10 in the southwest, with a distinct value of 29(°C) for G05. The annual minimum temperatureat the deposition siteswas also warmer than average with the exception ofG05, which experienced a minimum value of +2(°C) above zero.

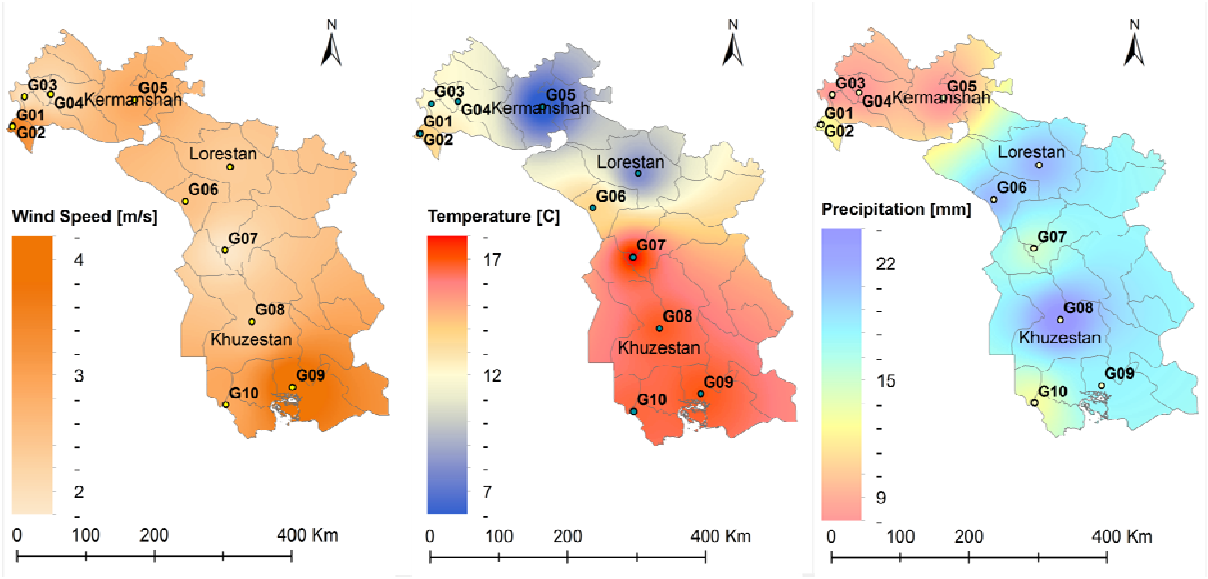

Fig. 4. Mapping meteorological data from the study area, 2014-2015.
**From left to right: Wind, Temperature, and Precipitation*

In general, the wind speed for the geographical area of study is shown in Fig. 4. A year's worth of wind speed data from March 2014 to 2015 shows that the highest wind speeds are found in the southern part of the study area, while the lowest speeds are found in the center part. the wind speed in the center part (G06, G07) was less than 3 (m s^{-1}) while it exceeded 4 (m s^{-1}) in the south (G09, G10) and extreme western parts (G01,G02, G03) of the research area.

3. METHODS AND DATA

It is important to measure the following two factors to understand the chemical characterization of aeolian dust deposition in the area of study. To begin with, measurement dependence of dust deposition rate, werefollowed by chemical analysis using inductively coupled plasma mass spectrometry (ICP-MS).

3.1 Measurement dependence of dust collection

Both gravimetric and directional dust samplers were constructed and installed from G01 to G10 at a 2 m height above ground (Fig. 5)to observe deposited particulate matter that settles from the air. The sampler design was deliberately kept simple to ensure long-term durability and easy maintenance[49][50]. Each sampler consisted of a plastic container with a surface area of 314 cm^2 (inverted Frisbee design) and a paper inlay for the passive dust collection.

a. Installment G01-G10 **b. Sample preparation**

Fig. 5. Installment and sampling technique

3.2 Chemical composition

The collected material was transferred into plastic bags on a monthly basis between March 2014 and March 2015 and was stored at room temperature before being analyzed using an ICP-MS[51]. After dust sample taken from the field, all extraneous material and particulate contaminants (insoluble pieces, high mass loading of surfactants, tissue, etc) removed from samples. The DIN EN ISO 17294-2 [52]; [53]guideline on quantifying dissolved elements using the ICP-MS was used for determining the elemental composition of the dust samples.Accurate measurement and identical process are done by weighing for one gram of each sample. Among the following four USEPA methods[54];[55](Tab. 3), method 3050 was deliberately chosen.

Table 3. Four digestion methods based on USEPA

Methods	Reagents	Digestive	Recoveries Strength
3050	HNO_3- HCl	Hotplate	-
3051	HNO_3	Microwave	-
3051A	HNO_3- HCl	Microwave	Zn Hg
3052	HNO_3- HCl- HF	Microwave	All elements except Pb – Mg

A representative 1 (gram)of each sample is digested with 15 and 5 (mL) respectively additions of Hydro-chloric and Nitric acid in 200 (mL) Flasks, closed using a vapor recovery glass left at the laboratory hood condition overnight. The samples cooked to 95(°C) ± 100(°C) without boiling over one hour until oxidation is finished. Then,digested samples arefiltered into the 50 (mL) volumetric-flask and diluted to a final volume of 50 (mL) with double deionized water. Finally, 1 (mL) of agents from previous step prepared in 10 (mL) Test-tube through ICP-MS process.The raw data from the instrument is depicted in (ppb)concentration (Tab. 4).

Table 4. Data relative to digestive samples

Run	Time	23Na (ppb)	24Mg (ppb)	28Si-3V (ppb)	39K-3V (ppb)	43Ca (ppb)	88Sr (ppb)	138Ba (ppb)	206Pb (ppb)
1	10:51:54	4.21	0.065	1.472	0.443	0.576	0.003	0.017	0
2	10:51:57	7.322	0.151	0.151	1.892	3.407	0	0.026	0
3	10:52:01	8.733	0.181	0.181	1.051	2.843	0.005	0.029	0
X		6.755	0.132	0.132	0.49	1.891	0	0.013	0
S		2.314	0.06	0.06	1.751	2.155	0.004	0.026	0
%RSD		34.26	45.5	45.5	356.9	113.9	831.2	202.3	0

As is shown above table, a part of raw data relative to digestive samples from our ICP-MS software; "X ", "S", and "RSD" represent average, standard deviation, and SD relative respectively.

The (ppb) data from the ICP-MS was printed out into an excel format. Each sample is analyzed three times, and the average of the three replicates was calculated, including means, and standard. Accuracy and precision in terms of RSD (%) which stands for relative standard deviation have been determined by the machine (ICP-MS: X series II). The process has been taken in a minute for each sample.

$$\%RSD = \frac{S(SD)}{X(mean)} \times 100$$

Equation.1

$$True\ value \underset{S(SD)}{\Leftarrow} RSD \times \left(\sum_{i=1}^{3} Na_i \right) / 3$$

Equation.2

Tab. 4 presents the acceptance criteria for Natrium [Na]. The %RSD value is calculated right 34.26 using equation Eq. (1). Mass true value on the other hands is taken from Eq. (2). Accuracy within the minimum and maximum value, therefore, are obtained from Eq. (3).

$$\min_{Na} value + \overline{\overline{True\,value}}^{SD} \cong \max_{Na} value - \overline{\overline{True\,value}}^{SD} \cong \left(\frac{X}{Na} \left| \left(\sum_{i=1} Na_i / 3 \right) \right. \right)$$

Equation.3

The result retrieved from ICP-MS is converted to the mass concentration metric using Eq. (4).

$$(ICP - MS^{ppb} \times Tm_1^{ml} \times Tm_2^{ml}) / \left(\overline{\overline{Pm_1^g \times Pm_2^{ml}}}^{Mass\ Product\ [I]\times[II]} \right) = \underset{Metric}{\overline{\overline{\text{Result}\ \mu g / kg}}}^{Interperting}$$

Equation.4

$$ICP - MS\ Measured\ (ppb)\ .\ Dilution\ (mL)\ /\ Weighting\ (g)\ =\ Interperting\ Result\ (\mu g / kg)$$

Equation. 5

Since our samples have been performed 2 dilutions, Interpreting Result (µgkg^{-1}) would be recalculated from the above equation and divided by 1000 unit to get final interpreted of (µg g^{-1}). Finally, the dilution information from the ICP-MS converted to value of (µg g^{-1}) out into an excel format (Tab.5).

Table 3. interpretation and mass calculation of elements

Dilution I g-mL	Dilution II g- mL	Run	23Na (ppb)	24Mg (ppb)	28Si-3V (ppb)	39K-3V (ppb)	43Ca (ppb)	138Ba (ppb)
Pm I=1	Pm II=1	X	6.755	0.132	0.132	0.49	1.891	0.013
Tm I=50	Tm II=10	$\boldsymbol{mg/L}$						
	Interpreted Result	3.377	0.066	0.066	0.245	0.9455	0.0065	

1 $\boldsymbol{\mu g/l = 1ppb}$

4. RESULTS AND DISCUSSION

Large correlation data sets of dust event history and deposition rate based on true-table are obtained per month. In with deposition rate and event history relation, correlation of chemical characteristics of samples addressed effect to aerosol from dominant and natural sourcesregarding Airborne Metal Regulation (AMR).

4.1 Contribution of wind aspects

The wind roses show the time ratio where winds blow from a particular direction at a certain speed (Fig. 6). To emphasize this dynamic, the direction has been marked using an external arc with a different color. Exterior red arcs from G01 to G10 illustrate that the maximized key-direction between 180 and 360 degrees comprised 50% to 100% of all monthly wind direction from northwest to southwest, with an exception at G08 where the wind almost altered 360 degrees at a maximum speed value of 2 (m s^{-1}). However, winds from eastern directions were rarely detected at a maximum speed value of 1 (m s^{-1})at G03, G04 and almost 2 (m s^{-1}) at G07 and G08. As shown in Fig.6, a strong key direction is indicated a speed value of 4 (m s^{-1})at G01 and G02 for southwest winds, while northwest winds were coupled with the same speed value at G09 and G10. In addition, winds from the north and west blew up to 3 (m s^{-1})at G06, whereas the same strong value for wind speed was also indicated at G07 from the west. The key-directions at G05 illustrated the wind blew up to 2 (m s^{-1}) from the northwest.

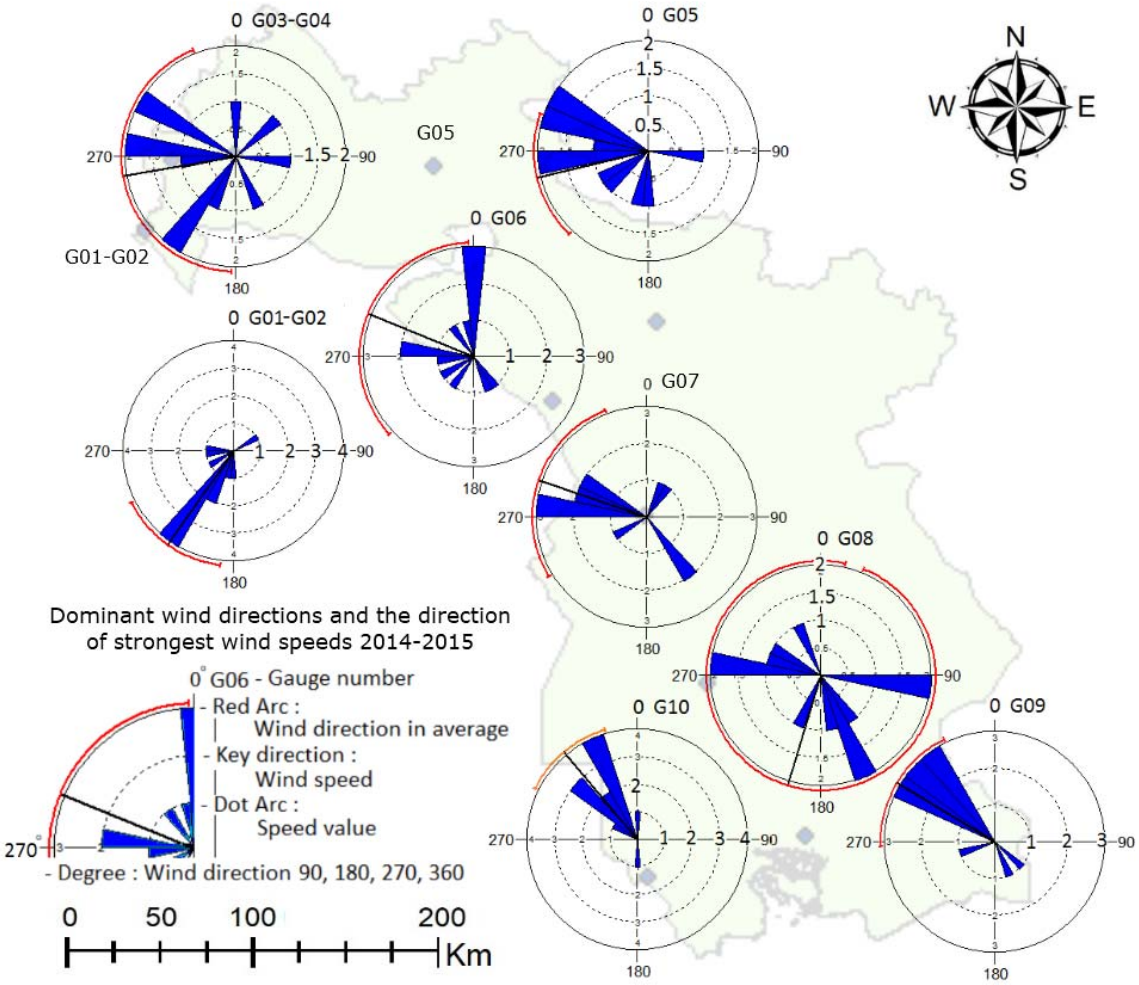

217 **Fig. 6. Wind rose speed and direction on data reproduced from IRMO**

218

219 **4.3 Deposition rate and dust event history**

220 Dust event frequency in concert with the deposition rateis represented in Tab. 6. While DEF values increased to
221 2, 3, or 5 times evidence of dust per month in the south and west, the DEF values at G05 and G06 were zero.
222 The high magnitude of DEF was observed in the south for G09 and G10 during January and February 2015.
223 The same values were also found in the west for G01 and G02 during March, April, and May 2014.
224 The average dust deposition rates ranged from 0.3 (mg cm-²) (G04-G06, Tab. 6) to 1.2 (mg cm-²)(G01), which
225 equals the monthly field deposition rates of 30-120 (kg ha^{-1}), while most stations, recorded a maximum between
226 2 and 3 (mg cm-²) (Tab. 6). Therefore, the correlation values of DEF and the observation report from the dust
227 deposition value can be considered. The monthly report from sites G01, G03, G04, G07, G08, G09, G10
228 indicated a strong correlation between DEF values and Dust Weight (Wt). Correlation magnitudes of 0.35, 0.49,
229 and 0.69 were indicated for the Wt numbers of G05, G02, and G08, respectively.

230

Table 4.Dust deposition rates vs dust event frequency(DEF)

Chronic		Sample sites G01-G10(mg cm-²)																			
Month	**Year**	**G01**	**DEF**	**G02**	**DEF**	**G03**	**DEF**	**G04**	**DEF**	**G05**	**DEF**	**G06**	**DEF**	**G07**	**DEF**	**G08**	**DEF**	**G09**	**DEF**	**G10**	**DEF**
Mar	2014	0.6	1	0.8	1	0.2	0	0.2	0	0.5	0	0.2	0	0.2	0	0.7	1	0.6	1	1.0	2
Apr	2014	2.6	4	2.0	3	0.5	1	~2	0	0.2	0	0.2	0	1.0	0	0.5	0	0.9	1	0.8	1
May	2014	1.0	2	~0.5	2	0.3	1	~3	0	0.3	0	0.1	0	0.5	0	0.2	0	0.5	0	0.2	0
Jun	2014	1.5	2	~0.8	2	0.8	1	0.2	0	1.0	0	0.2	0	0.5	1	0.6	1	1.0	1	1.0	1
Jul	2014	0.8	1	0.5	1	0.8	1	0.2	0	~0.9	0	0.3	0	0.6	1	1.9	1	1.2	1	0.9	1
Aug	2014	1.5	2	1.0	2	0.9	1	0.0	0	~2	0	0.6	0	0.3	1	~2	1	1.8	2	2.1	3
Sep	2014	1.5	2	1.5	2	0.9	1	0.5	0	~1	0	~15.9	0	0.2	0	0.6	0	0.9	1	0.9	1
Oct	2014	0.9	1	0.6	1	0.2	0	0.2	0	0.1	0	~9.5	0	0.2	0	0.3	0	0.3	0	0.3	1
Nov	2014	~2	0	0.9	0	0.2	0	0.2	0	0.1	0	1.0	0	0.2	0	0.2	0	0.5	0	0.2	0
Dec	2014	~1.5	0	0.2	0	0.1	0	0.2	0	0.2	0	0.2	0	~0.9	0	0.3	0	0.3	0	1.0	0
Jan	2015	1.8	2	1.0	2	0.8	1	0.6	1	0.2	0	0.3	0	2.5	3	2.0	3	2.5	4	3.1	5
Feb	2015	0.5	1	0.4	1	0.6	1	0.2	0	0.2	0	0.1	0	~1.7	0	0.8	1	1.5	1	1.1	1
Mar	2015	0.8	1	0.3	0	0.4	0	0.5	1	0.6	1	0.2	0	1.0	1	0.9	0	0.7	0	2.1	0
Average		1.20		0.80		0.50		0.30		0.30		0.30		0.70		0.80		1.00		1.10	
Min		0.50		0.20		0.10		0.00		0.10		0.10		0.20		0.20		0.30		0.20	
Max		2.60		2.00		0.90		3.00		2.00		15.9		2.50		2.00		2.50		3.10	
Total		17.0	19	10.5	17	6.7	8	8.0	2	7.3	1	28.8	0	9.8	7	11.0	8	12.7	12	14.7	16
Correlation		0.96		0.49		0.81		0.73		0.35		0.00		0.85		0.69		0.93		0.74	
P-Value<		0.05		0.05		0.05		0.05		NA		NA		0.05		0.05		0.05		0.05	
R Square		0,55		0.86		0.55		0.73						0.58		0.68		0.53		0.92	

**Dust deposition rates (Wt. in mg cm-²) and dust event frequency (DEF)in the gray columns (events/month) from the sites G01 to G10 during March 2014 and March 2015, as well as thePearson correlation for each station. Unusual values are highlighted in a "~"prefix,are removed from the calculation and are not influence on results.*

For all gauges site in red block, significant and correlation value are shown in Fig. 7. We note that more correlative data between the DEF and Wt were presented in April and May 2014 for G01 and G02 significantly with *P*=.001, and *P*=.004 Similarly, in with significant at *P*=.004, and *P*=.003 a high correlation value was observed during January and February 2015 at G09 and G10.

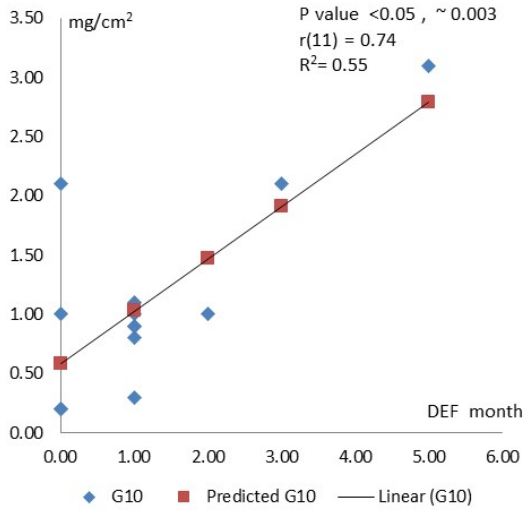

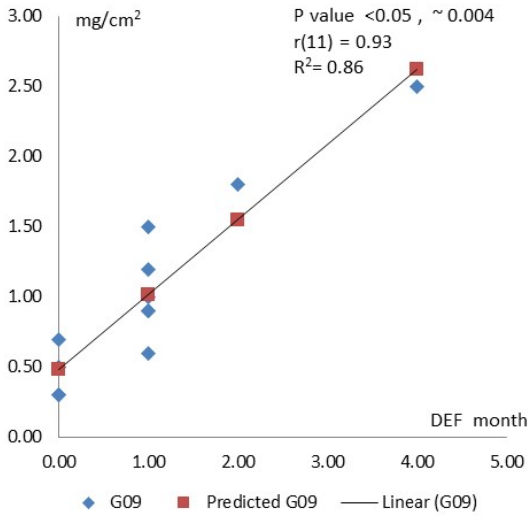

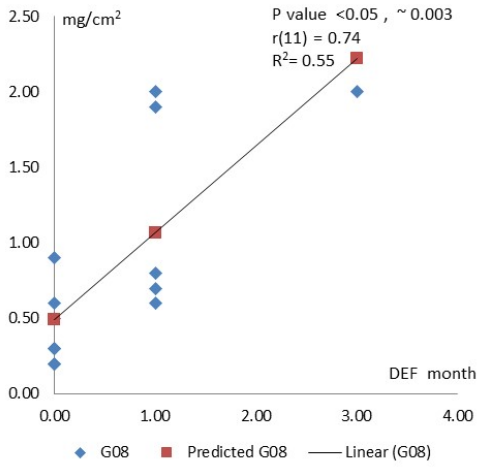

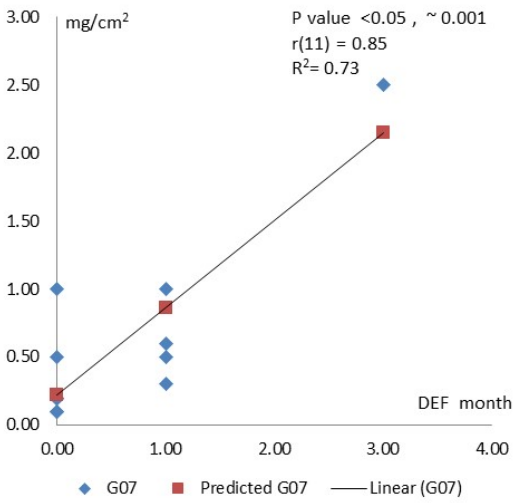

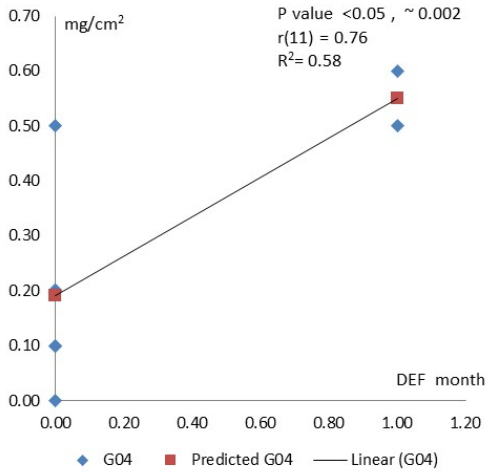

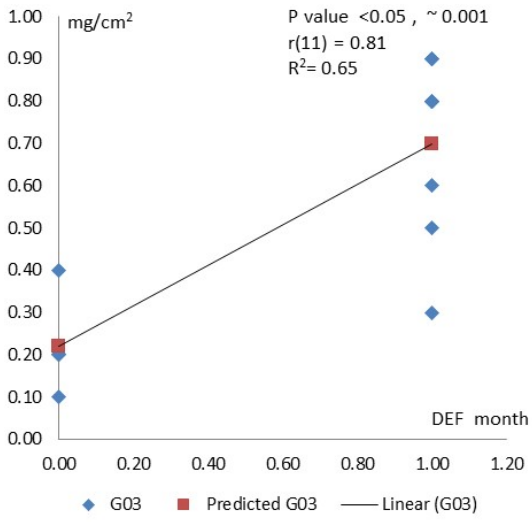

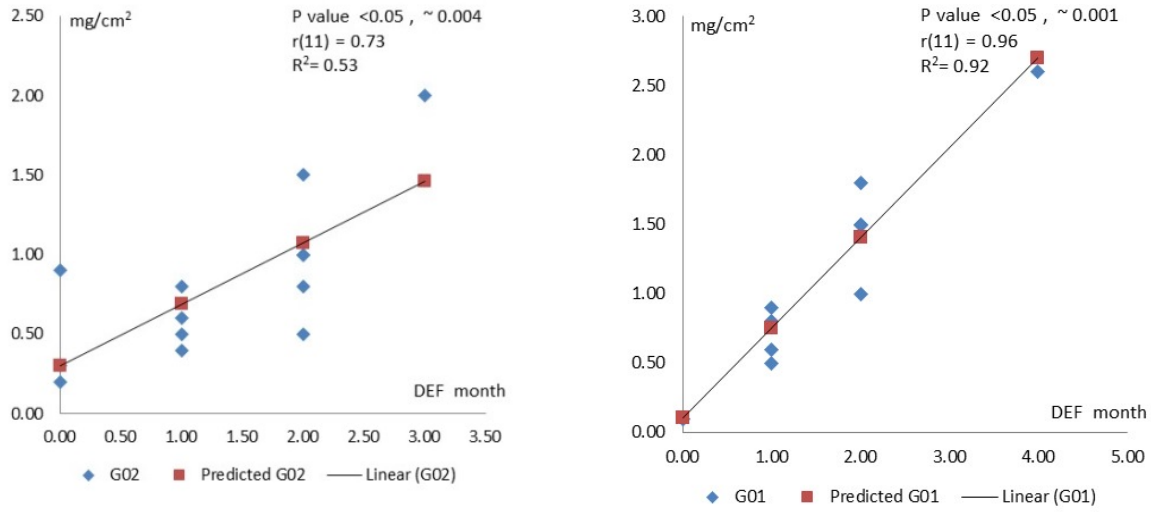

Fig. 7. Correlative data between the DEF (horizontal) and Wt (vertical)

**Predicted lines were presented in April and May 2014 for G01 and G02,January and February 2015 for G09and G10.*

4.4Chemical characterization of samples

Results from these ICP-MS analyses must be split into four groups to support the value and interpretation of the elements, as well as find any deviation from anthropogenic activities. As shown in Tab. 7, results from the characterized chemical value based on AMR were deployed through the measurement point to articulate the spatial and temporal classifications that were made by characterizing the chemical composition of particle matter.

Table 5.The total element concentrations inthe southern and western parts of the study area (in µg g^{-1})

Elements/ samples		*West-2014/01/04-05		*South-2015/01/01-02		Element concentrations (µg g^{-1})				
		W14104	W14105	S15101	S15102	Ave	S.D	Max	Min	Mean(SD)
Matrice	EF	3.42	2.00	4.87	1.15	1.34	1.16	4.87	0.00	1.34±1.16
AMR	Wt mg/cm^2	2.48	0.94	3.15	1.47	1.19	0.69	3.15	0.23	1.19±0.69
1	Na	4.23	2.97	5.13	1.28	4.20	1.79	9.12	1.28	4.20±1.79
	Mg	86.01	62.64	52.08	37.52	62.28	20.04	104.75	30.38	62.28±20.04
	Al	39.32	34.33	30.98	21.02	29.86	8.29	41.15	16.08	29.86±8.29
	Si	11.58	3.62	2.20	2.27	4.46	4.26	14.05	-0.06	4.46±4.26
	K	19.37	16.58	13.08	7.42	14.85	5.52	31.25	6.14	14.85±5.52
	Ca	694.62	554.38	235.30	147.70	400.91	238.83	725.00	110.50	400.91±238.83
	Mn	1.72	1.48	1.54	1.24	1.47	0.41	2.90	0.90	1.47±0.41
	Fe	92.57	77.23	75.92	56.99	70.98	18.30	98.45	43.00	70.98±18.30
	Sr	14.08	12.42	0.88	0.48	0.00	0.01	0.01	0.00	0.00±0.01
2	K	19.37	16.58	13.08	7.42	14.85	5.52	31.25	6.14	14.85±5.52
	Zn	2.04	0.00	5.29	1.15	1.74	1.61	5.29	0.00	1.74±1.61
3	Cr	0.43	0.17	0.24	0.15	0.29	0.13	0.65	0.11	0.29±0.13
	Fe	92.57	77.23	75.92	56.99	70.98	18.30	98.45	43.00	70.98±18.30
	Mg	86.01	62.64	52.08	37.52	62.28	20.04	104.75	30.38	62.28±20.04
	Co	0.05	0.05	0.04	0.03	0.04	0.02	0.10	0.01	0.04±0.02
	Ni	0.44	0.36	0.38	0.21	0.32	0.09	0.45	0.16	0.32±0.09
	V	0.15	0.15	0.12	0.11	0.15	0.05	0.30	0.08	0.15±0.05
4	Cu	0.22	0.08	0.16	0.10	0.15	0.06	0.30	0.08	0.15±0.06
	As	0.00	0.00	0.01	0.02	0.02	0.02	0.06	0.00	0.02±0.02
	Cd	0.01	0.01	0.05	0.05	6.92	6.39	14.17	0.43	6.92±6.39
	Ba	0.51	0.34	0.36	0.49	0.42	0.12	0.70	0.21	0.42±0.12
	Pb	0.05	0.05	0.21	0.05	0.08	0.05	0.21	0.03	0.08±0.05

**The next two digits number come after West (represented W) and South (represented S) likewise W14 and S15 are indicated an event in the west 2014 and south 2015 respectively. The next number "1" is shown the first day of each months followed by the last two digits in the west (04, 05) and south (01, 02) which are represented (April, May) and (Jan, Feb).AMR can be seenin the first column abbreviated of Airborne Metal Regulation, average as Ave, standard deviation as S.D., maximum as Max, and minimum as Min including plus/minus value for Means (SD).*

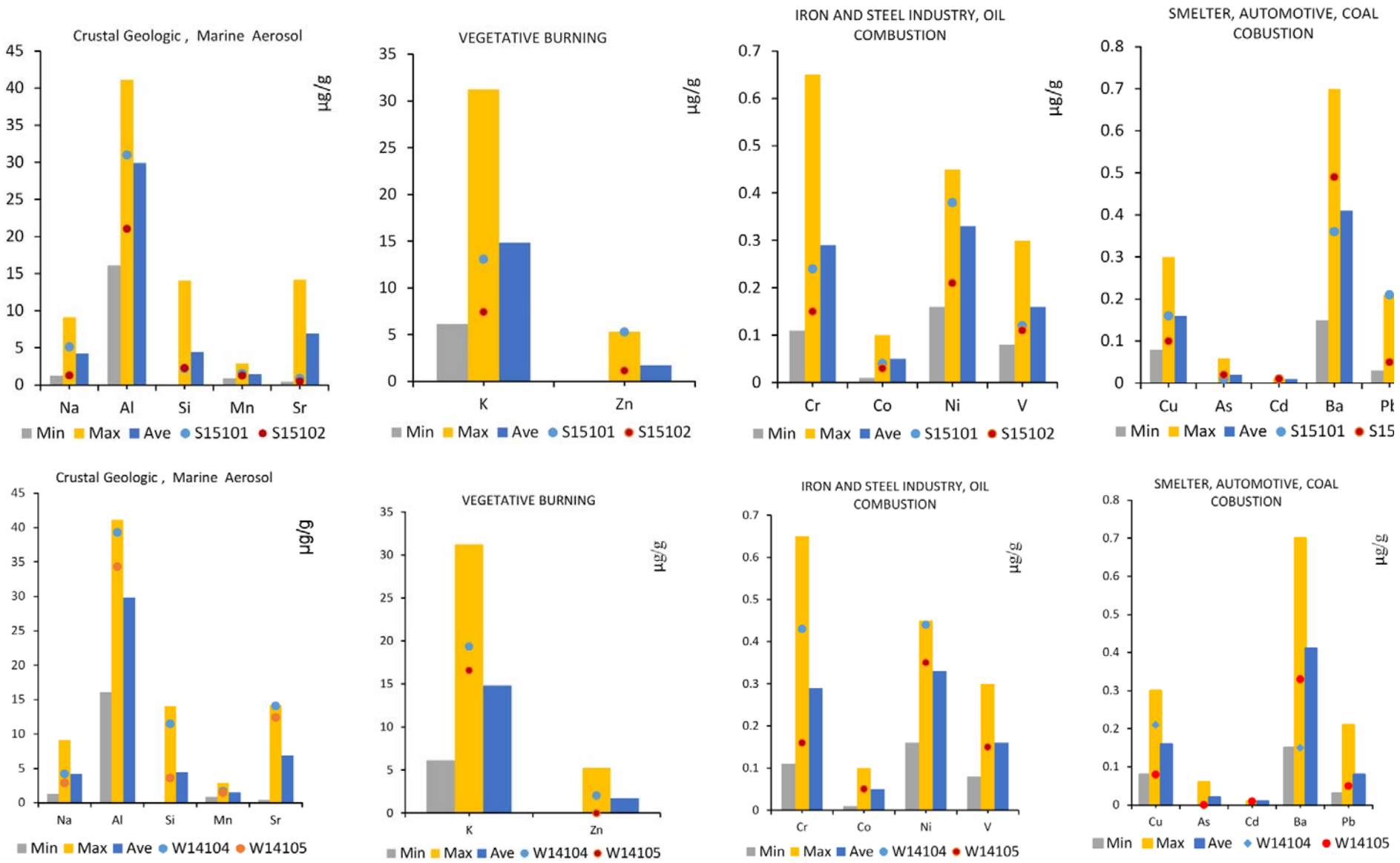

264 **Fig.8. Concentration value chart from the southern (top) and western (bottom) study area in four groups after Geiger and Cooper (2010) [left to righ**

As shown in Fig.8, from left to right, important to trace elements from crustal geologic sources were placed in the first group, vegetative burning sources were placed in the second group, iron and steel industry-coal combustion sources were placed in the third group, followed by smeltery, automotive and coal combustion sourcesin the final group.

The highest values (in µg g-1) of elements in the study area were obtained in April 2014 for Mg(86.10), Al(39.32), Si(11.58), K(19.37), Mn(1.72), Fe(92.57), and Sr(14.08) in the west however, in January 2015 the value for Na(5.13) was an exception to this finding in the southern study area.The minimum elemental levels in the southernpart of the study area were found for February 2015. Namely, minimum values (in µg g-1)are indicated forNa(1.28), Mg(37.52), Al(21.02), Si(2.20), K(7.42), Mn(1.24), Fe(56.99), and Sr(0.48).Although the elementconcentrations of the firstgroup are indicated as being below the maximum values, clearly above average valueswere nonetheless observed in the western part of the study area for this group; however, the values for Na, Al, Mn, K and Fe were exceptions to this finding, as they were equal to the average of all values in the southern study area.The ratio of standard deviation to average values for thisgroup is less than 50%, that is, 5:10, which is equivalent to the ratio 1:2.The bigger the value of the coefficient of variation represents the greater the level of dispersion around the means value, or make the less precise the estimate.

The minimum values (in µg g-1) of Zn(0, 1.1)and K(16, 7.42) in May and Februarywere observed in both the westernand the southern parts of the study area.Moreover, the maximum values (in $^{\mu g\ g\text{-}1}$) of K (19.37, 13) and Zn(2, 5.29) are observed in April and January in the same locations.Concordantly, the K values is revealed to be 3 times and 2 times above the minimum values (6.14) in April and May were observed in the western part of study area, whereas in the southern part the Zn value is equal to the maximum of all values in January. The coefficient of variance for vegetative burning is K(0.37) and Zn(0.92), that is, 37:100 for K and almost 1 for Zn. A remarkable increase inthe values of K and Zn may influence the deliberate burning of agricultural residues that occur in the southern part of the study area.

The impact caused bythe iron and steel industries, including emissions from oil combustion, influences the third group of Airborne Metals Regulations with attention to; Cr, Fe, Mg, Co, Ni, and V.The concentration of Cr bothin the western and southern parts of the study area has beenrevealed to be below average in May, January, and February.Instead,the observational value in the western part of the study areain April is an exception,with a substantially above average result of 0.43µg g-1.Further, the concentration magnitudeofFeand Niis increased byalmost a maximum of all values(92.57µg g-1and 0.44µg g-1, respectively) and islikely 30% above average in the western part. However, in the southern part, theyhardly pass the average in January and stayed below average in February.By the same token, the highest values for Mg(86.01µg g-1and 62.64µg g-1)areas above the average(61.72µg g-1) of all values in the western partin April and May.Moreover, the January and February concentrationswere not leveled up anygreater than average.Similarly, the concentration values (in µg g-1) of Co(0.04) and V(0.12)remain slightly below average in the south for January and February but above average in the west.Vanadium reaches the same value of average in April and May in the west.The ratio of the standard deviation to average values for the 3rd group is less than 40%, that is,4:10, which is equivalent to the ratio 2:5.

Smelter, Automotive, and Coal combustion sourcescomprise the fourth group.As has been noted, Cu(0.22µg g^{-1}) was almost 3 times above the minimum magnitude in April, although shortly after Cu(0.08µg g^{-1}) decreased the value by the minimum magnitude(0.08µg g^{-1}) and 50% of the average in May. In the south, however, Cu(0.16µg g^{-1}) showed an average value and was leveled by 50% of the maximum. Conversely, Cu(0.10µg g^{-1}) decreased the magnitude by 3 times below the maximum(0.30µg g^{-1}) in February. Near zero results were obtained for As and Cd in the west and the south. Moreover, the Ba(0.51µg g^{-1}) value in April isclose tothe average(0.42µg g^{-1}) magnitudebutwasnevertheless over double the minimum(0.21µg g^{-1}) in May.In January and February, the concentration values (in µg g^{-1}) of Ba(0.36and 0.49)were twice as largeas the minimum(0.21)and withdrawal average. In the same way,the maximum magnitude of Ba for all samplesremainedbelow(0.70).Although a steady magnitude was observed for Pb(0.05µg g^{-1}) in the west during April and May, in the south onlyPb(0.21µg g^{-1}) experienced amaximum value in January.

4.5 Chemical characterization and calculation

The correlation values of 20 elements to the DEF and its weight as based on the Airborne Metal Regulations index has been classified into four matrices. Correlation strength may be due to the exposure of aerosol and dust particles to extra elements throughout the dust's travel history. In either case, the correlation strength may be related to distance from the source, the wind direction, the meteorological situation, and industrial and commercial activities nearby.

As Tab. 8 shows, the strong uphill correlation in the western part of the study area is caused by geological influences that are dependent upon many factors from the DEF and Wt. A positive relationship is articulated from K and Fe to Al equally from Fe to K. In the same way, a strong positive correlation is represented among the elements of the first group, except for the moderate positive correlations from Si to Na (55%), Mg (66%), Al (53%), from Sr to Si (57%) and Mn (66%),and from Fe to Si (54%). To this end, weak but still positive correlations from Sr to Na (34%) and Mn to Si (49%) are recognized.A strong correlation magnitude is shown from K (73%) to the DEF and Wt, as well as a moderate positive correlation from Zn (50%) to dust weight.

There was a lack of correlation from Zn (18%) to DEF. In fact, no correlation is observed from Zn to elements from the first group such as: Mg (6%), Al (-14%), K (-10%), Ca (-9%), Mn (-7%), and Fe (8%). However, a weak

positive correlation is indicated for Na (33%) and Si (58%), and a weak negative correlation to Sr (-33%) is included.

A high correlation value is depicted in the 3rd group of Airborne Metals Regulations with a given strong correlation magnitude from DEF and Wt to Cr, Fe, Mg, Co, Ni, as well as an exception of a moderate positive relationship from V (53%). A perfect positive relationship can be seen between Fe and Ni to Al and K. Although a strong correlation value is given to K from the 2nd group, zero relationships are expressed from the group elements to Zn, albeit not for the weak correlation from Cr to Zn (58%).

As the same manner, there is a strong correlation from Cr (88%) to Si, a moderate correlation from Fe (54%), Ni (58%), and Mg (66%) to Si, and weak positive correlations from Co (42%) and V (31%) to Si. Moreover, a strong, positive individual correlation can be seen between Fe or Ni to Al and K. A strong positive relationship from Cu and Ba to DEFand the Wt. is revealed, excluding an uphill negative correlation from As and Cd (-82%) to the dust event frequency. At the same time, a moderate negative relationship is indicated from the Wt correlation for As (-56%) and Cd (-54%).

A strong positive relationship to Cu and Ba from the first, second and third groups can be recognized; however, there are negative relationships with As and Cd and a close to zero relationship with Pb. In addition to the negative relationships, a strong negative correlation can be seen between Ba to As and Cd. Notwithstanding the strong relationship of DEF and Wt. to the elements from matrices based on Airborne Metals Regulations, a moderate but positive correlation can be found to Na, Mn, Sr, Co, and V. Conversely, strong negative correlations are shown with As and Cd followed by near zero relationships to Zn and Pb.

In the southern study area (Tab. 9) correlation matrices of monthly concentrations represent strong uphill relation values from Na (76, 70%) and/or Sr (83, 93%) to DEFand Wt., respectively. Conversely, null and moderate negative relationship values occur with Ca (-8, -18%) and Si (-57, -74%). Similarly, a strong positive correlation is represented among the elements of the first matrix with an exception of a significant negative correlation to Sr (-93%). Furthermore, there are moderate negative relationships from Si to Mn (-45%), Fe (-43%), and Ca (-52%), and zero relationships are revealed from Si to Na (-5%), and Mg (-6%).

Positive relationships with DEF and Wtare articulated in the second matrix. Significantly positive correlation values are observed from K to Na (89%), Mg (97%), Al (92%), Ca (71%), Mn (84%), and Fe (86), as well as from Zn to Na (79%), and Sr (77%). The exceptions are an almost zero correlation to Ca (-100%) and a negative correlation to Si (-48%). Although a strong correlation is observed from Ni (71, 79%) and Fe (71%) to the DEFand Wt., in general, a moderate positive relationship characterizes the correlation from the third matrix to DEF and Wt. There are perfect positive relationships from Co to Al (100%), and from Fe to Mn (100%), while there are almost zero correlation states from Cr to Sr, and from Mg to Si. Weak to moderately negative relationships from V (14%), Ni (37%), Co (25%), and Fe (43%) to Si are shown.

The high correlation value is depicted from the final matrix to Wt values. Relationship values are strongly positive for Pb (95%) and Cu (72%). In contrast, strong negative correlations are shown with Cd (-73%), and As (-95%) with a weak positive correlation with Ba (33%). Correlations of the matrix to dust event frequency (DEF) show a perfect and moderate negative value to As (100%) and Cd (55%), respectively, and almost no relationship to Ba (7%). In contrast, strong and moderately positive values are articulated to Pb (99%) and Cu (64%), respectively.In addition to the relationship among elements and dust event frequency, no correlation was observed from Cu and As to Si and Ca, respectively. By the same token, zero correlation is expressed from Cd to Na, Mg, K, Co, and V. There was also zero correlation from Ba to Na, Ca, Zn and As. A strong negative correlation is also shown from As to Sr (-85%), Zn (-99%), from Pb to As (-98%), and from Cd to Sr (-92%). Weak negative correlations are shown from Cd to Al (-33%), Mn (-45%), Fe (-44%), Zn (-46%), and Ni (-36%). A moderate negative correlation is shown for Pb coupled with Ba to Si (50%), and Cd (50%).Aside from the moderate relationship of DEF and Wt to the matrices of the elements, a high positive correlation for these objects can be found with Fe, Sr, Zn, Ni, Cu, and Pb; conversely, an exceptional perfect negative correlation is found with As. Furthermore, a weak to near zero correlation can be seen with Ba, Ca and V.

Table 6. Key indicating elements with associated sources for maximum correlation in the westernstudy area 2014-2015

Capacitance measurement of dust

Var.	Elements (Correlation %)																						
West	DEF	Wt	Na	Mg	Al	Si	K	Ca	Mn	Fe	Sr	K	Zn	Cr	Fe	Mg	Co	Ni	V	Cu	As	Cd	Ba
DEF	1.00																						
Wt	0.92	1.00																					
Na	0.56	0.73	1.00																				
Mg	0.81	0.82	0.89	1.00																			
Al	0.75	0.70	0.84	0.98	1.00																		
Si	0.90	0.97	0.55	0.66	0.52	1.00																	
K	0.77	0.73	0.85	0.99	1.00	0.55	1.00																
Ca	0.92	0.82	0.68	0.94	0.93	0.71	0.94	1.00															
Mn	0.68	0.69	0.90	0.98	0.99	0.49	0.99	0.88	1.00														
Fe	0.75	0.73	0.87	0.99	1.00	0.54	1.00	0.93	0.99	1.00													
Sr	0.87	0.63	0.34	0.72	0.76	0.57	0.76	0.92	0.66	0.73	1.00												
K	0.77	0.73	0.85	0.99	1.00	0.55	1.00	0.94	0.99	1.00	0.76	1.00											
Zn	0.18	0.50	0.33	0.06	-0.14	0.58	-0.10	-0.09	-0.07	-0.08	-0.33	-0.10	1.00										
Cr	0.80	0.96	0.87	0.84	0.72	0.88	0.74	0.74	0.74	0.75	0.45	0.74	0.58	1.00									
Fe	0.75	0.73	0.87	0.99	1.00	0.54	1.00	0.93	0.99	1.00	0.73	1.00	-0.08	0.75	1.00								
Mg	0.81	0.82	0.89	1.00	0.98	0.66	0.99	0.94	0.98	0.99	0.72	0.99	0.06	0.84	0.99	1.00							
Co	0.71	0.60	0.73	0.93	0.98	0.42	0.98	0.93	0.96	0.97	0.81	0.98	-0.30	0.59	0.97	0.93	1.00						
Ni	0.78	0.75	0.85	0.99	1.00	0.58	1.00	0.95	0.99	1.00	0.77	1.00	-0.08	0.76	1.00	0.99	0.97	1.00					
V	0.53	0.53	0.86	0.91	0.96	0.31	0.95	0.79	0.98	0.96	0.57	0.95	-0.19	0.62	0.96	0.91	0.94	0.94	1.00				
Cu	0.77	0.95	0.88	0.84	0.71	0.87	0.74	0.72	0.74	0.75	0.42	0.74	0.60	1.00	0.75	0.84	0.58	0.75	0.62	1.00			
As	-0.82	-0.56	-0.30	-0.70	-0.75	-0.50	-0.75	-0.90	-0.65	-0.72	-1.00	-0.75	0.41	-0.38	-0.72	-0.70	-0.82	-0.75	-0.58	-0.36	1.00		
Cd	-0.82	-0.54	-0.25	-0.66	-0.71	-0.50	-0.71	-0.87	-0.61	-0.68	-0.99	-0.71	0.42	-0.36	-0.68	-0.66	-0.78	-0.71	-0.53	-0.33	1.00	1.00	
Ba	0.73	0.82	0.97	0.98	0.94	0.64	0.95	0.85	0.96	0.96	0.57	0.95	0.20	0.89	0.96	0.98	0.86	0.95	0.91	0.89	-0.54	-0.49	1.00
Pb	-0.42	-0.11	0.52	0.11	0.09	-0.27	0.09	-0.24	0.23	0.13	-0.58	0.09	0.29	0.17	0.13	0.11	0.00	0.08	0.33	0.21	0.58	0.62	0.29

AMR 1st AMR 2nd AMR 3rd AMR 4th

Strong and Perfect Relationship

Negative
Zero
Positive

Zero relationships. Up to 30%, A weak relationship. Up to 50%, A moderate relationship. Up to 70%, Strong and perfect relationship Up to 100

Table 7. Key indicating elements with associated sources for maximum correlation in the southern part of the study area, 2014-2015

Capacitance measurement of dust

	Var.		Elements (Correlation %)																				
South	DEF	Wt	Na	Mg	Al	Si	K	Ca	Mn	Fe	Sr	K	Zn	Cr	Fe	Mg	Co	Ni	V	Cu	As	Cd	Ba
DEF	1.00																						
Wt	0.95	1.00																					
Na	0.76	0.69	1.00																				
Mg	0.37	0.47	0.78	1.00																			
Al	0.57	0.69	0.80	0.96	1.00																		
Si	-0.57	-0.74	-0.05	-0.06	-0.33	1.00																	
K	0.47	0.50	0.89	0.97	0.92	0.04	1.00																
Ca	-0.08	-0.18	0.57	0.62	0.39	0.73	0.71	1.00															
Mn	0.51	0.68	0.67	0.92	0.98	-0.45	0.84	0.25	1.00														
Fe	0.55	0.71	0.72	0.93	0.99	-0.43	0.86	0.28	1.00	1.00													
Sr	0.83	0.93	0.38	0.22	0.49	-0.93	0.20	-0.52	0.54	0.55	1.00												
K	0.47	0.50	0.89	0.97	0.92	0.04	1.00	0.71	0.84	0.86	0.20	1.00											
Zn	0.99	0.92	0.79	0.37	0.54	-0.48	0.49	-0.01	0.46	0.51	0.77	0.49	1.00										
Cr	0.38	0.39	0.86	0.96	0.87	0.16	0.99	0.79	0.78	0.80	0.07	0.99	0.40	1.00									
Fe	0.55	0.71	0.72	0.93	0.99	-0.43	0.86	0.28	1.00	1.00	0.55	0.86	0.51	0.80	1.00								
Mg	0.37	0.47	0.78	1.00	0.96	-0.06	0.97	0.62	0.92	0.93	0.22	0.97	0.37	0.96	0.93	1.00							
Co	0.56	0.66	0.83	0.97	1.00	-0.25	0.95	0.47	0.96	0.97	0.43	0.95	0.54	0.91	0.97	0.97	1.00						
Ni	0.71	0.79	0.87	0.91	0.98	-0.37	0.91	0.36	0.94	0.96	0.58	0.91	0.69	0.85	0.96	0.91	0.98	1.00					
V	0.23	0.40	0.61	0.97	0.93	-0.14	0.88	0.50	0.94	0.93	0.22	0.88	0.21	0.87	0.93	0.97	0.93	0.85	1.00				
Cu	0.64	0.72	0.88	0.95	0.99	-0.27	0.95	0.46	0.94	0.96	0.48	0.95	0.63	0.91	0.96	0.95	0.99	0.99	0.89	1.00			
As	-1.00	-0.95	-0.73	-0.33	-0.54	0.59	-0.43	0.13	-0.48	-0.52	-0.85	-0.43	-0.99	-0.33	-0.52	-0.33	-0.52	-0.68	-0.20	-0.61	1.00		
Cd	-0.55	-0.73	-0.04	-0.06	-0.33	1.00	0.04	0.74	-0.45	-0.44	-0.92	0.04	-0.46	0.16	-0.44	-0.06	-0.25	-0.36	-0.15	-0.27	0.58	1.00	
Ba	0.07	0.35	0.16	0.67	0.72	-0.50	0.48	-0.03	0.84	0.80	0.38	0.48	-0.01	0.44	0.80	0.67	0.68	0.61	0.82	0.60	-0.05	-0.51	1.00
Pb	0.99	0.95	0.84	0.48	0.65	-0.50	0.59	0.05	0.58	0.62	0.78	0.59	0.99	0.50	0.62	0.48	0.65	0.78	0.34	0.73	-0.98	-0.48	0.11

AMR 1st AMR 2nd AMR 3rd AMR 4th

Strong and Perfect Relationship

Negative
Zero
Positive

Zero relationships. Up to 30%, A weak relationship. Up to 50%, A moderate relationship. Up to 70%, Strong and perfect relationship Up to 100

Henceforth, differential correlations between the southern and western parts of the study areafromSi, Ca, Al and MgtoDEF and Wt, as adjacent to local weathering (wind speed and wind direction, land cover based on Tab.2, discrimination of the first group elemental concentration value) suggest that: Si, Ca, Al and Mg may have higher local impactson the atmosphere rather than globally. Consequently, the nearby source contributors of the first matrix (Crustal Geologic and Aerosol Marine) should be monitored to predictthe concentration valuesof these elements within soil and water.As an illustration, the addition of Si decreased the values of Mn, Cu, Fe, and Zn. Moreover, some elements tend to be depleted (e.g., Zn, Fe, Cu, Mn) or enriched (e.g., Si, Mg, Na, K), which may occur as a result of soil weathering processes and anthropogenic factors.Meanwhile,the efficacy of Airborne Metal Regulations in the second matrix can be proven in the west and south parts of the study areaby revealing the lack of any strong correlation fromZn and K to DEFand Wt, respectively. Similarly, elemental values of Kalong with Zincdeficiency are related to the vegetative burning activities after or during the harvesting season.Although Chromium and Magnesium levels declined in the southern part of the study area, the contributions of iron-steel industries and oil combustion located therehave shown a proven disruption of correlation values in the 3rdmatrix. Thus,this relationship should be included in conversationsabout outcomes from anthropogenic activities and media from different geographical regionsregardless of concentration level.Notably, with Chromium, the concentrations of Vanadium areslightly elevated from oil combustion sources. Identically, the correlation amongelements from the 4thmatrix to the dust's physicalproperties shows a clear reduction in lead concentrations in the western part of the study area. Although at least two sites showa contribution of lead from industrial stations nearby, the only possible explanation for the overall reduction appears to be the absence of lead from industrial emissions. The concentrations of cadmium are low in the westand elevated in the south, which isprobably due to the wind direction and seasonal rains.

5. CONCLUSION

Dust events originate predominantly in arid or semiarid areas, and cover approximately 33% of the global land area [56] and 58% of the study area. The rates of dust deposition observed across the study area vary at almost250 gin square meters per year. The sites receiving dust deposition were classified into broad categories based on natural and anthropogenic features.The element concentration analysis is carried out with the help of anInductively Coupled Plasma-Mass Spectrometer (ICP-MS) for 20 elements. Geometric values for each element in the southern part (n=50) andthe western part (n=50) of the study areawere compared. Specifically, positive,zero and negative correlations among elements and the physical parameters of dust samples adjacent to thefour matrices of Airborne Metals Regulations are observed. This study comprises a perfect complement to the lessons learned from[24]; [25]in finding dust sources by using texture similarities in dust accumulation in the area of research(G01 to G02; G09 to G10). At the same time, correlations from atmospheric reports and DEFcan prove that the highest proportion of dust subjected to Airborne Metals Regulations associated with dominantsources (DS) are formed at local and regional scales rather than globally.

To summarize, weathering combined with anthropogenic change influences the composition of dust traveling from the source region to local deposition; however,this composition cannot be easily controlled. Although in some cases a severity in correlation without a resulting change in the value of the element compositionhas been observed, elemental correlations of individual matrices are nonetheless the marked effects of dominant sources. An impediment arises from the fact that there is no way to isolate each individual matrix orthe environment from the effects of either anthropogenic sources or natural weathering processes. Given this point, developing guidance on the priorities of expanding projects and preventative actions towards potential dust deposition from natural and dominant sources may be a subject of institutional interest.

ACKNOWLEDGMENT

I wish to acknowledge field work cooperation utilized by my best friends,experts back-home, and the scientific contributions made by Dr. Jens Hahn, Department of Geography; Koblenz University. Moreover, thanks to the professional laboratory assistance from Nils Jansen, Olga Schechtel and Nina Zitzer with regards to preparation and the operation of the instruments, respectively.

FUNDING SOURCES

This research didn't receive any specific grant from funding agencies in the public, commercial, or not-for-profit sector.

REFERENCE

1. D. ISO, “4225, 1996,” *Luftbeschaffenheit Ð Allg. Gesichtspunkte Begr. Beuth Berl.*
2. J. G. Calvert, “Glossary of atmospheric chemistry terms (Recommendations 1990),” *Pure Appl. Chem.*, vol. 62, no. 11, pp. 2167–2219, 1990.
3. J. M. Prospero, P. Ginoux, O. Torres, S. E. Nicholson, and T. E. Gill, “Environmental characterization of global sources of atmospheric soil dust identified with the Nimbus 7 Total Ozone Mapping Spectrometer (TOMS) absorbing aerosol product,” *Rev. Geophys.*, vol. 40, no. 1, 2002.
4. I. Tegen and A. A. Lacis, “Modeling of particle size distribution and its influence on the radiative properties of mineral dust aerosol,” *J. Geophys. Res.- Ser.-*, vol. 101, pp. 19–237, 1996.
5. J. Wu, Y. Xu, C. Fu, R. Zhang, M. Dai, and Y. Zhu, “Comparison of simulating mineral dust aerosols in East Asia by two emission schemes,” *China Particuology*, vol. 4, no. 06, pp. 293–299, 2006.
6. K. Carslaw *et al.*, “A review of natural aerosol interactions and feedbacks within the Earth system,” *Atmospheric Chem. Phys.*, vol. 10, no. 4, pp. 1701–1737, 2010.
7. G. S. Okin, N. Mahowald, O. A. Chadwick, and P. Artaxo, “Impact of desert dust on the biogeochemistry of phosphorus in terrestrial ecosystems,” *Glob. Biogeochem. Cycles*, vol. 18, no. 2, 2004.
8. N. M. Mahowald *et al.*, “Atmospheric global dust cycle and iron inputs to the ocean,” *Glob. Biogeochem. Cycles*, vol. 19, no. 4, 2005.
9. D. Goossens, B. Buck, and B. McLaurin, “Contributions to atmospheric dust production of natural and anthropogenic emissions in a recreational area designated for off-road vehicular activity (Nellis Dunes, Nevada, USA),” *J. Arid Environ.*, vol. 78, pp. 80–99, 2012.
10. J. Gillies, V. Etyemezian, H. Kuhns, D. Nikolic, and D. Gillette, “Effect of vehicle characteristics on unpaved road dust emissions,” *Atmos. Environ.*, vol. 39, no. 13, pp. 2341–2347, 2005.
11. B. Marticorena, G. Bergametti, D. Gillette, and J. Belnap, “Factors controlling threshold friction velocity in semiarid and arid areas of the United States,” *J. Geophys. Res. Atmospheres*, vol. 102, no. D19, pp. 23277–23287, 1997.
12. R. Reynolds, J. Belnap, M. Reheis, P. Lamothe, and F. Luiszer, “Aeolian dust in Colorado Plateau soils: nutrient inputs and recent change in source,” *Proc. Natl. Acad. Sci.*, vol. 98, no. 13, pp. 7123–7127, 2001.
13. J. Neff *et al.*, “Increasing eolian dust deposition in the western United States linked to human activity,” *Nat. Geosci.*, vol. 1, no. 3, p. 189, 2008.
14. I. Tegen, M. Werner, S. Harrison, and K. Kohfeld, “Relative importance of climate and land use in determining present and future global soil dust emission,” *Geophys. Res. Lett.*, vol. 31, no. 5, 2004.
15. N. M. Mahowald *et al.*, “Observed 20th century desert dust variability: impact on climate and biogeochemistry,” *Atmospheric Chem. Phys.*, vol. 10, no. 22, pp. 10875–10893, 2010.
16. W. G. N. Slinn, “Estimates for the long-range transport of air pollution,” *Water. Air. Soil Pollut.*, vol. 18, no. 1, pp. 45–64, Jul. 1982.
17. S. Visser and G. Sterk, “Nutrient dynamics—wind and water erosion at the village scale in the Sahel,” *Land Degrad. Dev.*, vol. 18, no. 5, pp. 578–588, 2007.
18. R. M. Williams, “A model for the dry deposition of particles to natural water surfaces,” *Atmospheric Environ. 1967*, vol. 16, no. 8, pp. 1933–1938, 1982.
19. W. Tao, J. Chen, Z. Li, C. Wang, and C. Zhang, “Impact of aerosols on convective clouds and precipitation,” *Rev. Geophys.*, vol. 50, no. 2, 2012.
20. B. Roth and K. Okada, “On the modification of sea-salt particles in the coastal atmosphere,” *Atmos. Environ.*, vol. 32, no. 9, pp. 1555–1569, 1998.
21. S. A. Morman and G. S. Plumlee, “The role of airborne mineral dusts in human disease,” *Aeolian Res.*, vol. 9, pp. 203–212, 2013.
22. H. Gerivani, G. R. Lashkaripour, M. Ghafoori, and N. Jalali, “The source of dust storm in Iran: a case study based on geological information and rainfall data,” *Carpathian J. Earth Environ. Sci.*, vol. 6, 2011.
23. N. Basta and S. McGowen, “Evaluation of chemical immobilization treatments for reducing heavy metal transport in a smelter-contaminated soil,” *Environ. Pollut.*, vol. 127, no. 1, pp. 73–82, 2004.
24. T. Larssen and G. Carmichael, “Acid rain and acidification in China: the importance of base cation deposition,” *Environ. Pollut.*, vol. 110, no. 1, pp. 89–102, 2000.

25. D. R. Muhs and J. B. Benedict, “Eolian additions to late quaternary alpine soils, Indian peaks wilderness area, Colorado front range,” *Arct. Antarct. Alp. Res.*, vol. 38, no. 1, pp. 120–130, 2006.

26. C. Opp, M. Groll, I. Aslanov, T. Lotz, and N. Vereshagina, “Aeolian dust deposition in the southern Aral Sea region (Uzbekistan): Ground-based monitoring results from the LUCA project,” *Quat. Int.*, 2016.

27. N. Ai and K. R. Polenske, “Socioeconomic impact analysis of yellow-dust storms: An approach and case study for Beijing,” *Econ. Syst. Res.*, vol. 20, no. 2, pp. 187–203, 2008.

28. A. Miri, H. Ahmadi, M. R. Ekhtesasi, N. Panjehkeh, and A. Ghanbari, “Environmental and socio-economic impacts of dust storms in Sistan Region, Iran,” *Int. J. Environ. Stud.*, vol. 66, no. 3, pp. 343–355, Jun. 2009.

29. W. Mertz, “The essential trace elements,” *Science*, vol. 213, no. 4514, pp. 1332–1338, 1981.

30. A. Kabata-Pendias, *Trace elements in soils and plants*. CRC press, 2010.

31. X. Wang, T. Sato, and B. Xing, “Size distribution and anthropogenic sources apportionment of airborne trace metals in Kanazawa, Japan,” *Chemosphere*, vol. 65, no. 11, pp. 2440–2448, 2006.

32. A. Geiger and J. Cooper, “Overview of Airborne Metals Regulations, Exposure Limits, Health Effects, and Contemporary Research,” *US Environ. Prot. Agency Accessed Accessed August*, vol. 25, p. 2015, 2010.

33. K. Schepanski, B. Heinold, and I. Tegen, “Harmattan, Saharan heat low, and West African monsoon circulation: modulations on the Saharan dust outflow towards the North Atlantic,” *Atmos Chem Phys*, vol. 17, no. 17, pp. 10223–10243, Sep. 2017.

34. “Global ambient air pollution,” World Health Organization, 2018.

35. M. J. Wilkinson, “The Persian Gulf, Clear and Clouded,” Johnson Space Center, Aug. 2014.

36. IRMO, “I.R.OF IRAN Meteorological Organization.” Dust National Center, 2016.

37. M. C. Peel, B. L. Finlayson, and T. A. McMahon, “Updated world map of the Köppen-Geiger climate classification,” *Hydrol. Earth Syst. Sci. Discuss.*, vol. 4, no. 2, pp. 439–473, 2007.

38. Statoids, “Administrative Divisions of Countries,” Montly Clearing House, Sep. 2016.

39. MCLSW, “GDP Report- The Provience Index,” Ministry of Cooperative labourand Social welfare, Annual Report, 2015.

40. Statistical Center of Iran, “National Population and Housing Census,” Vice Presidency Plan and Budget Organization Statistical Centre of Iran, Annual Report, Aug. 2018.

41. ASTER Science Team, “NASA EOSDIS Land Processes DAAC,” NASA/METI/AIST/Japan Spacesystems, and U.S./Japan, 2001.

42. J. T. Houghton, L. Meiro Filho, B. A. Callander, N. Harris, A. Kattenburg, and K. Maskell, “Climate change 1995: the science of climate change,” *Clim. Change*, p. 584, 1996.

43. K. Trenberth *et al.*, “Observations: surface and atmospheric climate change. Chapter 3,” *Clim. Change*, pp. 235–336, 2007.

44. H.-R. Adhami, B. Mesgarpour, and H. Farsam, “Herbal Medicine in Iran,” *HerbalGram J. Am. Bot. Counc.*, vol. 74, pp. 34–43, 2007.

45. A. Khalili and J. Rahimi, *Climate*. 2018.

46. Khosro Movahed, “Badgir (wind catcher) an example of traditional sustainable architecture for clean energy,” *2016 IEEE Smart Energy Grid Engineering (SEGE)*, pp. 79–83, 2016.

47. “Climate Change Knowledge Portal,” Climatic Research Unit (CRU) University of East Anglia (UEA), The World Bank Group, 2016.

48. Iran Meteorological Organization, “Precipitation Map,” 2014.

49. ASTM D1356, “Standard Terminology Relating to Sampling and Analysis of Atmospheres,” in *Book of Standards*, Subcommittee D22.03, 2017.

50. IHS under license with ASTM, “Standard Terminology Relating to Sampling and Analysis of Atmospheres,” *IHS License ASTM*, 2010.

51. ASTM D7439, “Standard Test Method for Determination of Elements in Airborne Particulate Matter by Inductively Coupled Plasma–Mass Spectrometry,” in *Book of Standards*, Subcommittee D22.03, 2014.

52. Beuth, “Wasserbeschaffenheit - Anwendung der induktiv gekoppelten Plasma-Massenspektrometrie (ICP-MS),” *2005-02*, no. DIN EN ISO 17294-2, 2004.

53. EN ISO 17294-2, “Water quality: Application of inductively coupled plasma mass spectrometry (ICP-MS).” Beuth Verlag GmbH, 2016.

54. Y. J. A. B. da Silva, C. W. A. do Nascimento, and C. M. Biondi, “Comparison of USEPA digestion methods to heavy metals in soil samples,” *Environ. Monit. Assess.*, vol. 186, no. 1, pp. 47–53, Jan. 2014.

55. M. Chen and L. Q. Ma, “Comparison of Three Aqua Regia Digestion Methods for Twenty Florida Soils,” *Soil Sci Soc Am J*, vol. 65, pp. 491–499, 2001.

56. R. Duce, “Sources, distributions, and fluxes of mineral aerosols and their relationship to climate,” *Aerosol Forcing Clim.*, vol. 6, pp. 43–72, 1995.